12-2008

Hydrodynamic loading of microcantilevers oscillating near rigid walls

Ryan C. Tung
Purdue University - Main Campus, rtung@purdue.edu

Jana Anirban
Purdue University - Main Campus

Arvind Raman
Birck Nanotechnology Center, Purdue University, raman@purdue.edu

Hydrodynamic loading of microcantilevers oscillating near rigid walls

Ryan C. Tung,[a] Anirban Jana,[b] and Arvind Raman[c]
School of Mechanical Engineering, Birck Nanotechnology Center, Purdue University, West Lafayette, Indiana 47907, USA

(Received 12 July 2008; accepted 15 October 2008; published online 5 December 2008)

The vibrations of microcantilevers in atomic force microscopes (AFMs) or radio frequency (RF) switches are strongly influenced by the viscous hydrodynamics of the surrounding fluid in the vicinity of a rigid wall. While prior efforts to model this hydrodynamic loading have focused on squeeze film damping effects at high Knudsen and squeeze numbers, the regimes of low Knudsen and squeeze numbers are also very important for which squeeze film models need to be discarded in favor of unsteady Stokes hydrodynamics. We extend the work of Green and Sader [Phys Fluids **17**, 073102 (2005); J. Appl. Phys. **98**, 114913 (2005)] and present compact semianalytical formulas for the unsteady viscous hydrodynamic function of slender microbeams oscillating near rigid walls, in terms of key nondimensional numbers. Using these closed-form expressions, it becomes possible to predict easily the wet natural frequencies and quality factors of multiple modes of microcantilevers near rigid walls in diverse applications ranging from AFM in liquids to RF microswitches under ambient conditions. The semianalytical formulas are extensively validated by comparing their predicted wet natural frequencies and quality factors with those based on three-dimensional, transient flow-structure interaction simulations, as well as previous experiments performed in the field by other researchers. © *2008 American Institute of Physics*.
[DOI: 10.1063/1.3033499]

I. INTRODUCTION

The hydrodynamic loading of microcantilever resonators is of great interest to the microelectromechanical system (MEMS) community. Of particular interest are the hydrodynamic loading of atomic force microscope (AFM) probes and radio frequency (RF) switches moving in a viscous fluid near a solid surface.[1] For example, the hydrodynamic damping of microcantilevers adversely affects imaging forces and sensitivity especially on soft biological samples.[2] For RF switches hydrodynamic damping influences the impact velocity and wear at the contact interface, and also the switch bounce.[3] An *a priori* knowledge of the quality factors and resonant frequencies of such resonators in fluidic environments is crucial for their effective design and operation.

This paper focuses primarily on microcantilevers oscillating in a viscous fluid near a wall under ambient temperature and pressure that fall within the low Knudsen and squeeze number regimes. The Knudsen number, defined as $\mathrm{Kn}=\lambda^*/H^*$ where λ^* is the mean free path for the fluid molecules and H^* is the gap between the beam and the wall, measures the degree to which the noncontinuum nature of the fluid is important. A low Knudsen number ($\mathrm{Kn}\leq 0.001$) signifies that the fluid can be treated as a continuum. The squeeze number, defined as $\sigma=12\mu_f^*\omega^* b^{*2}/(H^{*2}P_0^*)$ where μ_f^* is the dynamic viscosity of the fluid, ω^* is the angular frequency of the beam, P_0^* is the ambient pressure, and H^* is the gap height, measures the degree of compression in the fluid. A low squeeze number means that compressibility effects of the fluid are negligible. The low Knudsen and squeeze number regimes for microcantilever resonators are important because they are directly applicable to AFM probes oscillating in fluids at ambient pressure with significant gap, as well as to many RF switches under ambient conditions.

In our applications of interest the oscillations of the microbeam are small and the nonlinear convective fluid inertia terms in the Navier–Stokes equation are negligible, allowing us to use the unsteady Stokes equation. Using unsteady Stokes hydrodynamics provides the opportunity to develop hydrodynamic loading theories that are uniformly valid for large gaps tending to structures oscillating in unbounded fluid on one hand, and small gaps with strong squeeze film effects on the other hand. In contrast, squeeze film models such as those of Langlois,[4] Griffin *et al.*,[5] Blech,[6] Darling *et al.*,[7] Gallis and Torczynski,[8] and Veijola *et al.*[9] all rely on different versions of the Reynolds lubrication equation, and are not directly applicable to arbitrary gap heights. Unsteady Stokes hydrodynamics for long slender oscillating structures was mainly developed by Tuck,[10] who provided semianalytical solutions for a long, slender beam vibrating in an unbounded fluid with small amplitude. More recently Green and Sader[11,12] extended Tuck's[10] method to include the hydrodynamic effects introduced by a nearby surface. Clarke *et al.*[13–15] also calculated the drag on microcantilevers using two- and three-dimensional unsteady Stokes hydrodynamics. Furthermore, Clark and Paul[16] used a stochastic approach to calculate the damping of a microcantilever in a viscous fluid near a wall. However, these recent works do not provide a convenient way or an expression to calculate the hydrodynamic loading on the microbeam and instead require extensive computation.

[a]Electronic mail: rtung@purdue.edu.
[b]Electronic mail: janaanir@ecn.purdue.edu.
[c]Electronic mail: raman@purdue.edu.

In this paper we extend the theoretical techniques used by Tuck[10] and Green and Sader[11,12] to develop *semianalytical* solutions for the hydrodynamic loading of slender microbeams oscillating close to a rigid wall that are easy and convenient to use. Using these semianalytical expressions it becomes possible to predict the quality factors and natural frequencies of multiple modes of microcantilever beams near rigid walls in diverse low Knudsen and squeeze number applications ranging from AFM in liquids to RF microswitches under ambient conditions. For several microcantilevers, we also compare these theoretically predicted quality factors with those based on detailed three-dimensional finite element based computational fluid dynamics simulations, as well as existing experimental data. To the best of our knowledge, this is the first validation of the theory of Green and Sader[11,12] for microcantilevers oscillating close to a wall. From the above comparison, we see that the theory makes good predictions of the quality factors when the gap between the microcantilever and the wall is greater than a certain minimum threshold. For smaller gaps, the theoretical predictions start to diverge from the experimentally measured quality factors.

II. THEORY

In this section we briefly outline the theory of Tuck[10] and Green and Sader.[11,12] Figure 1(a) shows a typical microbeam system immersed in a fluid and near a rigid wall, together with the relevant dimensions and the coordinate system. We begin with the following assumptions.

(1) The beam is long, thin, and of uniform cross section.
(2) The beam oscillates transversely with an amplitude that is small compared to its width b^* and gap H^*.
(3) The fluid is incompressible and viscous.
(4) The axial flow velocity, as well as all gradients in the axial direction, is negligible.

These assumptions allow for the analysis of the flow in the two-dimensional plane containing the cross section of the beam as shown in Fig. 1(b).

Given the small fluid velocities in typical microcantilever resonators, such as AFM probes and RF switches, the nonlinear convective fluid inertia is negligible compared to the viscous fluid stresses. Under such conditions the fluid flow is governed by the unsteady Stokes and the continuity equation. We adopt a nondimensional Fourier transformed version of the unsteady Stokes and the continuity equation

$$i\,\mathrm{Re}\,\mathbf{u} = -\nabla p + \nabla^2\mathbf{u}, \quad \nabla\cdot\mathbf{u} = 0, \tag{1}$$

where distances are nondimensionalized by the cantilever half width $b^*/2$, the fluid velocity is nondimensionalized as $\mathbf{u}=u\mathbf{j}+v\mathbf{k}=\mathbf{u}^*/(b^*\omega^*)$, and the fluid pressure is nondimensionalized as $p=2\mu_f^*\omega^*p^*$. The nondimensional number Re $=\rho_f^*\omega^*b^{*2}/(4\mu_f^*)$ is the ratio of the unsteady fluid inertia to the viscous fluid stresses, and is often called the unsteady Reynolds number in literature. Note that we use asterisks to denote dimensional quantities.

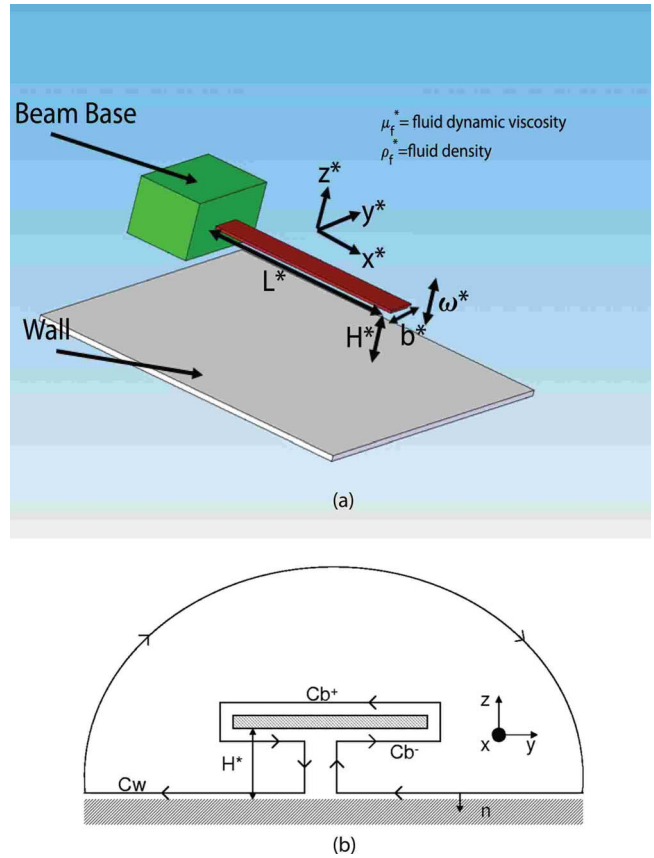

FIG. 1. (Color online) Schematic of a microcantilever immersed in a fluid near a rigid wall. L^* is the cantilever length, b^* is the cantilever width, H^* is the gap height, and ω^* is the frequency of oscillation. The coordinate system is fixed relative to the wall. (b) shows the two-dimensional cross section of the cantilever beam. C_{b+} and C_{b-} describe the contour around the top and bottom of the beam, respectively. C_w describes the contour along the wall.

For the low Knudsen number range that we consider here, the boundary conditions at solid-fluid interfaces can be assumed to be the classical no-slip boundary conditions. Thus, we have

$$u = 0, \quad v = 0 \quad \text{on} \quad z = 0 \ \ (\text{wall}),$$

$$u = 0, \quad v = V_b \quad \text{on} \quad z = H \ \ (\text{beam}), \tag{2}$$

where V_b is the transverse velocity amplitude of the beam cross section.

Next, following Tuck[10] and Green and Sader,[11] we reformulate the problem by introducing a stream function $\psi(y,z|\omega)$ such that $\psi_{,z}=u$ and $-\psi_{,y}=v$, where $(\ )_{,y}$ denotes differentiation with respect to y and so on. In terms of the stream function, the boundary conditions in Eq. (2) become

$$\psi_{,z}(y,0) = 0, \quad \psi_{,y}(y,0) = 0, \quad \psi_{,z}(y,H) = 0, \quad \text{and} \quad \psi_{,y}(y,H) = V_b. \tag{3}$$

Furthermore, using the divergence theorem and Green's identities, the stream function can be expressed as

$$\psi(y,z|\omega) = \int_{-\infty}^{\infty} [\zeta^w(y',0|\omega)\Xi_{,z'}(y',0|y,z) - p^w(y',0|\omega)\Xi_{,y'}(y',0|y,z)]dy' + \int_{-1}^{1} [\Delta\zeta^b(y',H|\omega)\Xi_{,z'}(y',H|y,z) - \Delta p^b(y',H|\omega)\Xi_{,y'}(y',H|y,z)]dy', \quad (4)$$

where ζ^w is the fluid vorticity at the wall, p^w is the pressure at the wall, $\Delta\zeta^b = \zeta^b_{\text{top}} - \zeta^b_{\text{bottom}}$ is the vorticity jump across the beam, and $\Delta p^b = p^b_{\text{top}} - p^b_{\text{bottom}}$ is the pressure jump across the beam. Finally, $\Xi(y,z|y',z')$ is Green's function for the operator $\nabla^4(\cdot) - i\,\text{Re}\,\nabla^2(\cdot)$,

$$\Xi(y,z|y',z') = \frac{1}{2\pi i\,\text{Re}}[K_0(\sqrt{iRe}R) + \log R], \quad (5)$$

where K_0 is the modified Bessel function of the third kind[17] and $R = \sqrt{(y-y')^2 + (z-z')^2}$. The system of four coupled integral equations arising from substituting the expression for ψ from Eq. (4) in the boundary condition (3) is solved numerically for the unknown pressures and vorticities. The numerical procedure is described briefly in Sec. III.

III. NUMERICAL PROCEDURE

The four coupled integral equations are first discretized using a numerical scheme similar to the one used by Tuck[10] and Green and Sader.[11] For the discretization, a nonuniform grid with nodes at (y_j, H), where $y_j = -\cos(\pi j/N)$, $j = 0,1,\ldots,N$, is employed to divide the width of the beam into N unequal elements. Additionally, the infinite wall is replaced with a wall of finite extent from $(-L_w, 0)$ to $(L_w, 0)$, albeit with the wall's extent chosen to be much greater than the beam width ($L_w \gg 1$). The finite wall is also segmented into N unequal elements using a nonuniform grid with nodes at $(L_w y_j, 0)$, $j = 0,1,\ldots,N$. This type of nonuniformity of the grids possesses a square root bias toward the edges, which mitigates the effect of the square root singularity of the pressure at the edges. The discretization is then carried out by (i) requiring the integral equations to be exactly satisfied at the midpoints of the beam and wall elements, (ii) rewriting each of the integrals over the beam and the wall as a sum of integrals over the individual elements, and (iii) simplifying the integrals over the individual elements by assuming that the unknown pressures and vorticities are constant over each element and equal to their values at the element midpoints. This discretization results in the following linear system of $4N$ algebraic equations in as many unknowns:

$$A_1\bar{\zeta}^w + A_2\Delta\bar{\zeta}^b - A_3\Delta\bar{P}^b = 0, \quad (6a)$$

$$B_1\bar{P}^w - A_3\Delta\bar{\zeta}^b + B_3\Delta\bar{P}^b = 0, \quad (6b)$$

$$C_1\bar{\zeta}^w - C_2\bar{P}^w - C_3\Delta\bar{\zeta}^b = 0, \quad (6c)$$

$$-C_2\bar{\zeta}^w + D_2\bar{P}^w - D_3\Delta\bar{P}^b = \bar{V}_b, \quad (6d)$$

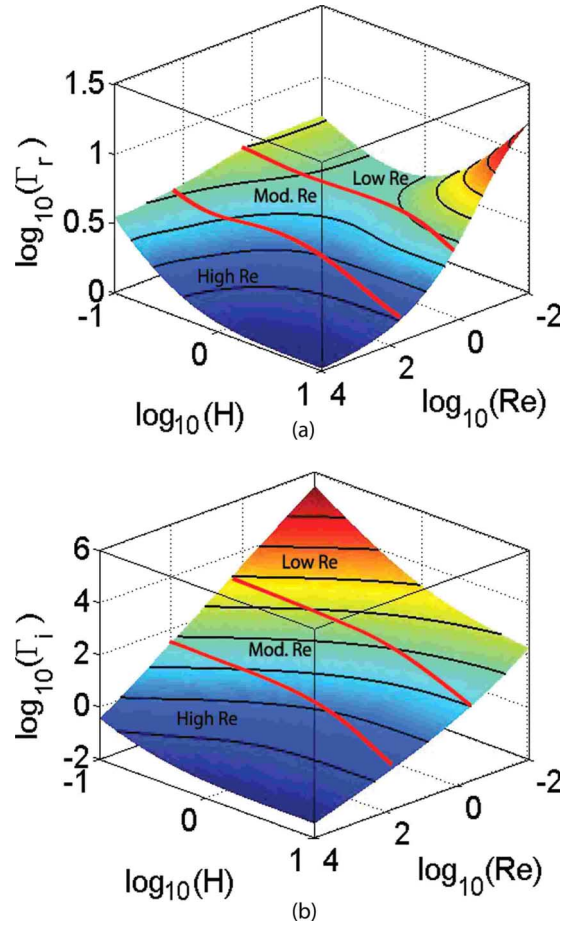

FIG. 2. (Color online) Hydrodynamic function Γ as a function of the unsteady Reynolds number, Re, and the nondimensional gap, H, computed based on the Tuck–Green theory. (a) shows the real part of Γ and (b) shows the imaginary part of Γ. The red lines divide the parameter space into regions of high, moderate, and low Re.

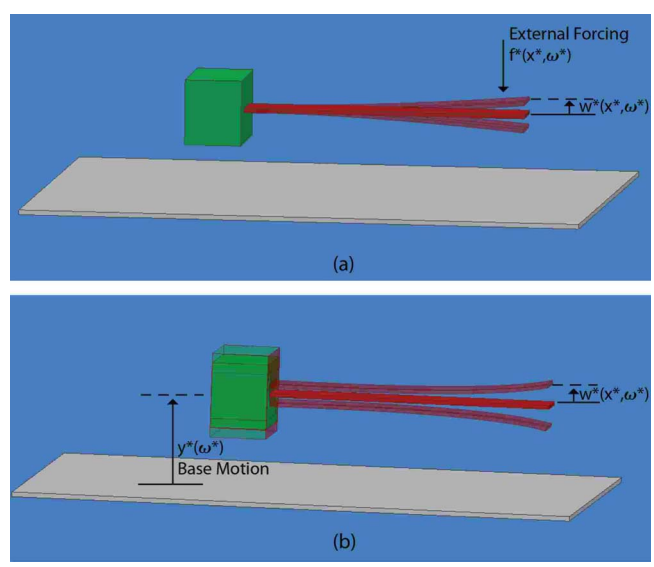

FIG. 3. (Color online) Two different excitation mechanisms for which the semianalytical expression for Γ can be used to predict the FRF. In (a) the microcantilever is held at a fixed distance from a rigid wall, and is excited by means of external fields such as magnetic or electrostatic forces as in magnetic mode AFM and RF switches. In (b) the microcantilever is excited inertially by means of a dither piezo at its base, as in acoustic mode AFM.

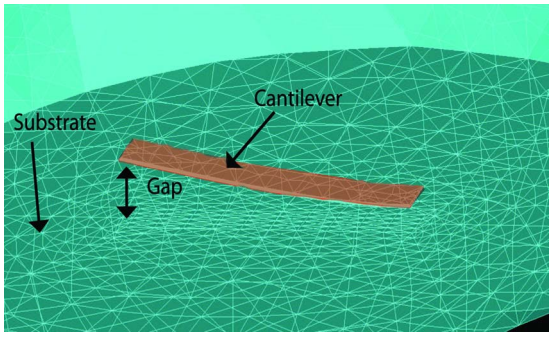

FIG. 4. (Color online) The computational mesh employed in the three-dimensional FSI simulations in ADINA.

where $\bar{\zeta}^w$ and $\bar{P}^w$ are the $N\times 1$ vectors of the unknown pressures and vorticities at the centers of the wall elements, $\Delta\bar{P}^b$ and $\Delta\bar{\zeta}^b$ are the $N\times 1$ vectors of the unknown pressure and vorticity jumps across the beam at the centers of the beam elements, and $\bar{V}_b$ is the $N\times 1$ vector of the known beam velocities at the centers of the beam elements. A_k, B_k, C_k, and D_k are $N\times N$ complex matrices, whose entries involve integrals of the derivatives of Green's function $\Xi(y,z|y',z')$ over the wall and beam elements. Green and Sader[11] provided closed-form analytical expressions for the entries of all these submatrices except A_2 and C_1. They computed the entries A_2 and C_1 via numerical quadrature, and so do we. In addition, since the closed-form formulas provided by Green and Sader[11] for the entries of A_1 and C_3 are very complicated, we compute these also by numerical quadrature. We employ the n-point Gauss–Legendre quadrature for constructing A_2, C_1, A_1, and C_3. The entries of all remaining submatrices are computed analytically.

Once all the submatrices are constructed, linear system (6) is solved in MATLAB. From the extracted pressure jump across the beam, the nondimensional hydrodynamic force on the beam can be computed as

$$f_{\text{hydro}} = -\int_{-1}^{1} \Delta p^b(y)dy \approx \sum_{j=1}^{N} \Delta\bar{P}_j^b(y_j - y_{j-1}). \tag{7}$$

An extensive convergence study was performed in order to obtain the optimum values for the number N of wall and beam elements, the wall length L_w as defined previously, and the order n of the Gauss–Legendre quadrature used for computing the entries of some of the submatrices. These optimum values need to be chosen such that the discretization and numerical errors are sufficiently small and the computational cost is not exceedingly high. The convergence study revealed that values of $n=10$, $N=500$, and $L_w=15$ are the optimum choices, for which the computational cost is reasonable, and the errors in the computed hydrodynamic forces are less than 1% for all values of the nondimensional gap H and the unsteady Reynolds number Re under consideration.

IV. COMPACT CORRELATIONS FOR THE HYDRODYNAMIC FUNCTION

Rather than directly present the computed hydrodynamic forces, we present the computational results in terms of the hydrodynamic function Γ,[10,11] defined as

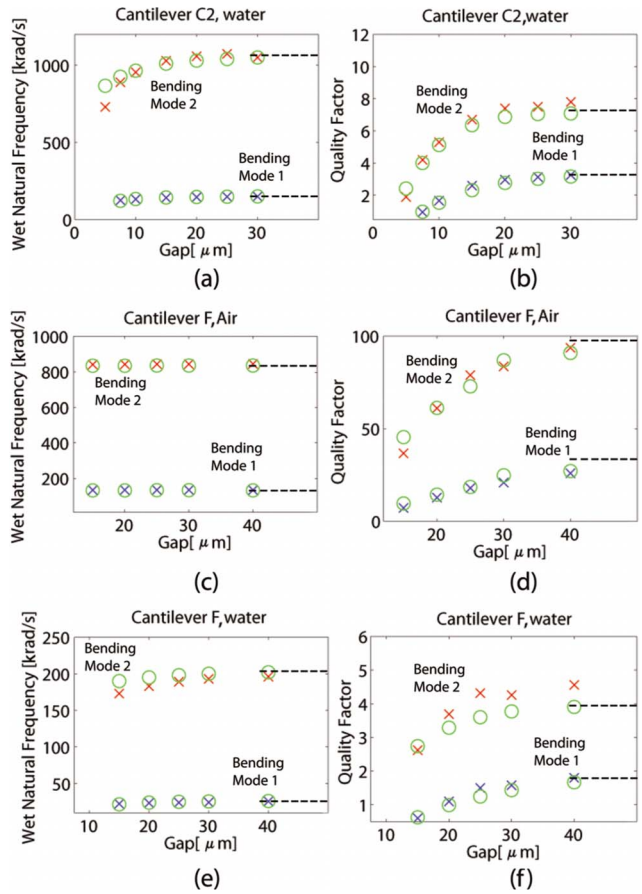

FIG. 5. (Color online) Plot showing the semianalytical predictions and those of the three-dimensional fluid structure interaction simulation performed using ADINA. Parts (a), (c), and (e) show the wet natural frequencies of the cantilever C2 in water, and cantilever F in air and water, respectively. Parts (b), (d), and (f) show the quality factors of the cantilever C2 in water, and cantilever F in air and water, respectively. All calculations are performed for ambient temperature and pressure. The circles represent the semianalytical predictions, while the crosses are the predictions based on the ADINA simulations. The dashed lines represent the asymptotic limit as the gap is increased infinitely, as in Ref. 10.

$$\Gamma(\text{Re},H) = \frac{i}{\pi\,\text{Re}} f_{\text{hydro}}. \tag{8}$$

The hydrodynamic function is a complex quantity that only depends on the unsteady Reynolds number Re and the nondimensional gap H. The imaginary part of the hydrodynamic function represents the fluid damping, while the real part represents the added mass effect of the surrounding fluid. Since the hydrodynamic function is dependent on only two nondimensional variables (Re and H) it is possible to accurately and conveniently describe the hydrodynamic loading of both AFM microcantilevers and RF switches under ambient conditions with the use of only two parameters.

The hydrodynamic function was then computed over a wide range of values of the unsteady Reynolds numbers, $\text{Re}\in[10^{-2},10^{4}]$, and the nondimensional gap, $H\in[0.1,10]$, each consisting of 40 points equally spaced in log space. The resulting two-dimensional surfaces of the real and imaginary parts of the hydrodynamic function are shown in Fig. 2. By way of example, a soft AFM microcantilever of width 30 μm oscillating in its first eigenmode at a resonance fre-

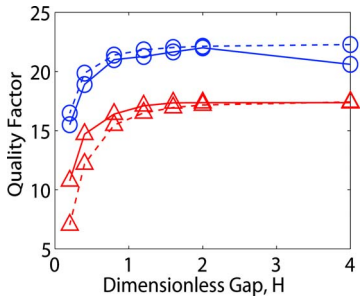

FIG. 6. (Color online) Comparison between the experimental measurements of Naik *et al.*(Ref. 20) and the predictions based on our semianalytical formula, for the second bending mode of the Bimorph® cantilever in two different Flourinert™ liquids, and at varying gap heights. Circles and triangles represent Fluourinert™ liquids FC-40 and FC-70, respectively. Data points connected by broken lines represent the semianalytical predictions, while those connected by solid lines represent the experimental measurements of Naik *et al.* (Ref. 20).

quency of 5 kHz in water at a gap of 5 μm (approximately the tip length of such AFM probes) possesses an unsteady Reynolds number of approximately 8 and a nondimensional gap of $H=0.3$. In contrast, a millimeter sized cantilever of width 1 mm oscillating in its first eigenmode at a resonance frequency of 2.9 kHz in air at a gap of 1 mm possesses an unsteady Reynolds number of approximately 300 and a nondimensional gap of $H=1$. If the hydrodynamic loading of higher eigenmodes is of interest then the angular frequency, ω, increases and the Re becomes larger. Clearly the chosen range of Re and H values covers a wide range of situations for AFM probes and RF switches.

Because it is difficult to find compact correlations that are uniformly valid over the entire range of Re and H computed, we instead choose to break up the results into three Re regimes: (a) the *low* Re regime, $10^{-2}<\mathrm{Re}<5$, (b) the *moderate* Re regime, $5<\mathrm{Re}<800$, and (c) the *high* Re regime, $800<\mathrm{Re}<10^4$. For each of the above Re regimes, $10^{-1}<H<10^1$. For example, typical soft AFM microcantilevers oscillating in air or water in the first bending mode would lie in the low Re regime, while AFM microcantilevers or RF switches oscillating in air in higher eigenmodes could lie in the moderate Re or high Re regimes depending on the frequency. In each of the above regimes a linear least-squares fit is performed on the computed hydrodynamic function data. The resulting closed-form compact correlations for the real and imaginary parts of the hydrodynamic function Γ in terms of Re and H for the three Re regimes are provided in the Appendix. We find that over the vast parameter space considered here, these closed-form expressions reproduce the computed data to within 10% at most, and typically within 3% for most of the parameter space.

V. PREDICTION OF WET RESONANCE FREQUENCIES AND *Q*-FACTORS USING THE COMPACT CORRELATIONS

In order to use the correlations in the Appendix to predict the resonance frequency and quality factor of different modes of a microbeam oscillating close to a rigid wall, first the correct transfer function between the input forcing and structural response needs to be identified. For instance, in Fig. 3, we show two typical situations in which a microcantilever close to a rigid wall may be excited and its response measured. In the first case [Fig. 3(a)], the cantilever is excited by external fields alone, as might happen for electrostatically actuated RF switches or for magnetically excited AFM microcantilevers. The corresponding frequency response function (FRF) can be shown to be[18]

TABLE I. Comparison between the experimental measurements of Naik *et al.*(Ref. 20) and the predictions based on our semianalytical formula. For these results, the nondimensional gap $H=2$.

		Wet natural frequencies (kHz)			Quality factors		
Fluid	Eigenmode	Expt.	Semianalytical	%Diff.	Expt.	Semianalytical	%Diff.
Air	1st bending	2.9	2.92	−0.590%	23	23.04	−0.154%
	2nd bending	18.6	18.29	1.672%	24	23.82	0.770%
	3rd bending	50.6	51.22	−1.215%	36	35.12	2.448%
FC-72	1st bending	2.43	2.50	−2.844%	19	21.43	−12.797%
	2nd bending	15.6	15.50	0.641%	23	25.06	−8.964%
	3rd bending	42.7	42.46	0.564%	31	37.35	−20.473%
FC-77	1st bending	2.44	2.48	−1.475%	18	19.83	−10.151%
	2nd bending	15.6	15.49	0.705%	22	24.04	−9.285%
	3rd bending	42.7	42.81	−0.260%	31	35.74	−15.304%
FC-40	1st bending	2.41	2.45	−1.502%	17	17.01	−0.039%
	2nd bending	15.5	15.44	0.394%	22	22.13	−0.581%
	3rd bending	42.3	43.08	−1.832%	29	32.98	−13.739%
FC-70	1st bending	2.41	2.39	0.797%	11	11.41	−3.695%
	2nd bending	15.5	15.26	1.574%	17	17.17	−1.002%
	3rd bending	42.1	42.97	−2.055%	24	25.89	−7.863%

$$\frac{w^*(\omega^*,x^*=L^*)}{f^*(\omega^*)}=\frac{\frac{1}{m^*}\Phi_n(L^*)\int_0^{L^*}\Phi_n(x^*)dx^*}{\left[\omega_n^{*2}-\omega^{*2}-\frac{\pi}{4m^*}\rho_f^*\omega^{*2}b^{*2}(\Gamma_r-i\Gamma_i)+i\omega^*c_0^*\right]\int_0^{L^*}\Phi_n^2(x^*)dx^*}, \tag{9}$$

where $w^*(\omega^*,x^*=L^*)$ is the tip displacement relative to the base, $f^*(\omega^*)$ is the amplitude of external forcing per unit length, ω^* is the forcing frequency, m^* is the mass per unit length of the beam, x^* is the lengthwise coordinate along the beam as defined in Fig. 1, ω_n^* is the natural frequency of the nth bending mode of the beam, $\Phi_n(x)$ is the corresponding modeshape normalized such that $\Phi_n(L^*)=1$, c_0^* is the coefficient of structural damping of the beam, and $\Gamma_r(\mathrm{Re},H)$ and $\Gamma_i(\mathrm{Re},H)$ are the magnitudes of the real and imaginary portions of the hydrodynamic function that need to be determined from the Appendix. In the second case [Fig. 3(b)], an AFM microcantilever can be excited inertially by means of a dither piezo in the vicinity of a substrate. For this situation, the FRF is given by

$$\frac{w^*(\omega^*,x^*=L^*)}{y^*(\omega^*)}=\frac{\left[\omega^{*2}+\frac{\pi}{4m^*}\rho_f^*\omega^{*2}b^{*2}(\Gamma_r-i\Gamma_i)\right]\Phi_n(L^*)\int_0^{L^*}\Phi_n(x^*)dx^*}{\left[\omega_n^{*2}-\omega^{*2}-\frac{\pi}{4m^*}\rho_f^*\omega^{*2}b^{*2}(\Gamma_r-i\Gamma_i)+i\omega^*c_0^*\right]\int_0^{L^*}\Phi_n^2(x^*)dx^*}, \tag{10}$$

where $y^*(\omega^*)$ is the amplitude of the absolute base displacement, and the other variables are as defined previously. These FRFs are valid in the vicinity of resonance of a specific eigenmode.

The aforementioned FRFs can be computed using the Re-regime dependent correlations for $\Gamma_r(\mathrm{Re},H)$ and $\Gamma_r(\mathrm{Re},H)$ provided in the Appendix. From the FRFs the *wet natural frequency* (or the frequency when immersed in fluid near the rigid wall) can be easily calculated. Furthermore the Q-factor of that mode can be determined from the FRF by using the half-power method.

VI. VALIDATION

To validate the accuracy of the semianalytical formulas (Appendix), their predicted Q-factors and resonance frequencies of different eigenmodes at varying gaps are compared to the following: (a) the computational results of Basak *et al.*,[19] (b) our own fully three-dimensional transient fluid-structure interaction (FSI) simulations, and (c) the experimental data of Naik *et al.*[20]

First, we compare the predictions based on our semianalytical formulas with those based on the computational results of Basak *et al.*,[19] and our own results to lower Reynolds numbers. Both sets of computations use the commercially available finite element package called ADINA (Ref. 21) to perform fully three-dimensional transient FSI simulations of the ringdowns of a number of different cantilevers immersed in different fluids and at various gaps above a rigid wall. Figure 4 shows the computational mesh. The details of the computational setup, along with the numbers and types of solid and fluid elements chosen, can be found in Ref. 19. Each ringdown simulation is initiated by imposing on the undeflected cantilever, a transverse velocity field with a spatial distribution corresponding to one of its structural modeshapes. The time history of the cantilever tip displacement from each ringdown is analyzed to obtain the corresponding modal wet natural frequency and quality factor. Note that the ADINA models do not incorporate any structural damping ($c_0^*=0$).

Figures 5(a) and 5(b) compare the wet natural frequencies and quality factors predicted by the semianalytical formula and the ADINA FSI simulations for the first and second bending modes of the cantilever C2 (Ref. 19) (whose dimensions are $197\times29\times2\ \mu\mathrm{m}^3$), oscillating in water at room temperature, and at various gap heights. Here $\mathrm{Re}\in(10^1,10^3)$. Figures 5(c)–5(f) present the same comparison for a rectangular silicon cantilever with dimensions $250\times25\times1\ \mu\mathrm{m}^3$ (which we label cantilever F), oscillating in air and water under ambient conditions. Here $\mathrm{Re}\in(10^{-1},10^2)$. In the above figures, the wet natural frequencies and quality factors of the cantilevers when they are very far away from the rigid wall (Tuck[10]) are also plotted. Clearly the quality factors and wet natural frequencies predicted using the semianalytical formula for $\Gamma(\mathrm{Re},H)$ agree closely with those based on the ADINA simulations for all values of Re and H considered above. A maximum error of 6.5% exists between the semianalytical and ADINA-based predictions for the quality factors, while a maximum error of 19% exists for the wet natural frequencies. The greatest discrepancies are observed for the quality factors corresponding

TABLE II. Values of the coefficients in the semianalytical formula for the hydrodynamic function.

	$\mathrm{Re}=10^{-2}-5$		$\mathrm{Re}=5-800$		$\mathrm{Re}=800-10^{4}$	
	Real	Imaginary	Real	Imaginary	Real	Imaginary
a_1	0.447563	1.166451	0.454992	1.048232	0.115690	−0.055778
a_2	−0.128094	−0.939118	−0.123600	−0.671922	0.041530	−0.052844
a_3	−0.026524	0.041405	−0.050658	−0.167450	0.000631	−0.042005
a_4	0.015513	0.006618	0.030315	0.096639	−0.011091	−0.022982
a_5	0.004567	−0.000518	−0.004347	−0.012839	0.001875	0.004113
a_6	−0.162957	0.205767	−0.199080	0.414505	−0.042464	−0.116570
a_7	0.037071	−1.480452	0.053699	−1.621577	−0.216779	−0.647854
a_8	0.291576	1.084622	0.196494	1.122649	0.153418	0.541078
a_9	−0.094668	0.043579	−0.143066	0.294719	−0.077252	−0.482199
a_{10}	−0.100082	−0.214250	−0.049848	−0.228261	−0.040086	−0.021487
a_{11}	−0.083228	0.127148	0.003749	0.159247	0.050556	0.206033
a_{12}	0.017776	0.066614	0.033247	0.110112	0.025747	0.090325
a_{13}	−0.015890	−0.033979	0.070494	−0.430455	0.012889	0.055147
a_{14}	0.024807	−0.005172	0.001729	−0.038745	−0.003101	−0.010253
a_{15}	0.017239	0.022154	0.006254	−0.086469	−0.006375	−0.058274
a_{16}	−0.010929	0.017535	−0.004849	0.025019	−0.001033	0.001208

to the second bending mode. This is mainly because the axial flow in the gap, which was neglected in developing the semianalytical formulas, becomes increasingly important for higher modes; other effects deleterious to our results include gradients in the axial direction and boundary layer growth, which again become increasingly important for higher modes.

Finally, comparisons of the predictions of our semianalytical formulas with the experimental data of Naik *et al.*[20] were also performed. In Ref. 20, Naik *et al.* measured the dynamic response of a Bimorph® cantilever ($10\times1\times0.5$ mm^3) experimentally in air and in Flourinert™ liquids with varying viscosities (but almost similar densities). Experimental procedures and material properties for Flourinert™ can be found in Ref. 20. In comparing with their experimental data, some care must be taken to account for the structural damping of their microcantilever. This is done by setting c_0^* in the FRFs (9) and (10) equal to its measured value (based on the cantilever's response in vacuum[20]).

Table I compares the semianalytical and experimental wet natural frequencies and quality factors for the first, second, and third bending modes of the Bimorph® cantilever,[20] oscillating in air and four different Flourinert™ liquids, at a *fixed* nondimensional gap of $H=2$. The semianalytical predictions are in close agreement with the experimental measurements of Ref. 20. The semianalytical and experimental wet natural frequencies agree to within 3%. The semianalytical and experimental quality factors agree to within 10% for most cases, with the maximum disagreement ≈20%. Again, the disagreement tends to be the maximum for the highest mode (third bending). Finally, Fig. 6 compares the semianalytical and experimental wet natural frequencies and quality factors for the second bending mode of the Bimorph® cantilever in Fluourinert™ liquids FC-40 and FC-70, for varying nondimensional gaps. Again, the two sets agree quite favorably, except at very small gaps. At very small gaps ($\mathrm{Kn}>0.001$), the number of fluid molecules in the gap becomes sufficiently small to give rise to noncontinuum effects such as slip at the solid boundaries. Such effects are expected to decrease the hydrodynamic damping and increase the quality factors. Since the semianalytical formula does not account for any noncontinuum effects, its predicted quality factors should be less than those measured experimentally at very small gaps, which is consistent with the trend observed in Fig. 6.

Overall, the predictions of our compact semianalytical formulas derived from two-dimensional unsteady Stokes flow are in close agreement with those based on fully three-dimensional FSI simulations, and experimental measurements, for a number of cantilever bending modes, many different fluidic environments, and a large range of unsteady Reynolds numbers and gap heights.

VII. CONCLUSIONS

This paper investigates the hydrodynamic loading of microcantilevers oscillating in a fluid close to a rigid wall, under the conditions of low Knudsen and squeeze numbers. The hydrodynamic function for such cantilevers is computed based on the two-dimensional Tuck–Green theory for a large range of unsteady Reynolds numbers and gap heights. Compact semianalytical formulas for the hydrodynamic function are extracted based on these computations. Using these semianalytical formulas, researchers can easily and accurately estimate the wet natural frequencies and quality factors for microcantilever resonators immersed in various fluids, including such diverse applications as AFM probes and RF-MEMS switches. Tuck–Green theory and our semianalytical formulas based on it are extensively validated by comparing with fully three-dimensional FSI simulations as well as experiments.

ACKNOWLEDGMENTS

The authors also acknowledge financial support for this research from the Sandia National Laboratories under Con-

tract No. 623235, "Fluid-structure interactions in microsystems."

APPENDIX

The general form of the semianalytical formula for the hydrodynamic function Γ is

$$\Gamma(\mathrm{Re},H) = 10^{\Gamma_L}, \tag{A1}$$

where

$$\begin{aligned}\Gamma_L(\mathrm{Re}_L,H_L) = {} & a_1 + a_2\mathrm{Re}_L + a_3\mathrm{Re}_L^2 + a_4\mathrm{Re}_L^3 + a_5\mathrm{Re}_L^4 \\ & + a_6\mathrm{Re}_L H_L + a_7 H_L + a_8 H_L^2 + a_9 H_L^3 + a_{10} H_L^4 \\ & + a_{11}\mathrm{Re}_L H_L^2 + a_{12}\mathrm{Re}_L^2 H_L + a_{13}\mathrm{Re}_L H_L^3 \\ & + a_{14}\mathrm{Re}_L^3 H_L + a_{15}(\mathrm{Re}_L H_L)^2 + a_{16}(\mathrm{Re}_L H_L)^3,\end{aligned}$$

$H_L = \log_{10}(H)$, and $\mathrm{Re}_L = \log_{10}(\mathrm{Re})$. The coefficients $a_k, k = 1,2,\ldots,16$ are complex valued. They are tabulated in Table II.

[1] C. Rankl, V. Pastushenko, F. Kienberger, C. M. Stroh, and P. Hinterdorfer, Ultramicroscopy **100**, 301 (2004).
[2] S. Hu and A. Raman, Appl. Phys. Lett. **91**, 123106 (2007).
[3] P. G. Steeneken, T. G. S. M. Rijks, J. T. M. van Beek, M. J. E. Ulenaers, J. D. Coster, and R. Puers, J. Micromech. Microeng. **15**, 176 (2005).
[4] W. E. Langlois, Q. Appl. Math. **20**, 131 (1962).
[5] W. S. Griffin, H. H. Richarson, and S. Yamanami, ASME J. Basic Eng. **88**, 451 (1966).
[6] J. J. Blech, ASME J. Lubr. Technol. **105**, 615 (1983).
[7] R. Darling, C. Hivick, and J. Xu, Sens. Actuators, A **70**, 32 (1998).
[8] M. A. Gallis and J. R. Torczynski, J. Microelectromech. Syst. **13**, 653 (2004).
[9] T. Veijola, H. Kuisma, and R. Lahdenperäa, Sens. Actuators, A, **48**, 239 (1995).
[10] E. O. Tuck, J. Eng. Math. **3**, 29 (1969).
[11] C. P. Green and J. E. Sader, Phys. Fluids **17**, 073102 (2005).
[12] C. P. Green and J. E. Sader, J. Appl. Phys. **98**, 114913 (2005).
[13] R. J. Clarke, S. M. Cox, P. M. Williams, and O. E. Jensen, J. Fluid Mech. **545**, 397 (2005).
[14] R. J. Clarke, O. E. Jensen, J. Billingham, A. P. Pearson, and P. M. Williams, Phys. Rev. Lett. **96**, 050801 (2006).
[15] R. J. Clarke, O. E. Jensen, J. Billingham, and P. M. Williams, Proc. R. Soc. London, Ser. A **462**, 913 (2006).
[16] M. T. Clark and M. R. Paul, J. Appl. Phys. **103**, 094910 (2008).
[17] *Handbook of Mathematical Functions*, edited by M. Abramowitz and I. A. Stegun (Dover, New York, 1972).
[18] X. Xu and A. Raman, J. Appl. Phys. **102**, 034303 (2007).
[19] S. Basak, A. Raman, and S. V. Garimella, J. Appl. Phys. **99**, 114906 (2006).
[20] T. Naik, E. K. Longmire, and S. C. Mantell, Sens. Actuators, A **102**, 240 (2003).
[21] ADINA R & D Inc., ADINA 8.3 manuals, www.adina.com, Watertown, MA, 2005.